HHS Public Access

Author manuscript

J Physiol. Author manuscript; available in PMC 2022 December 01.

Published in final edited form as:

J Physiol. 2021 December ; 599(23): 5229–5242. doi:10.1113/JP281964.

T1ρ imaging as a non-invasive assessment of collagen remodeling and organization in human skeletal muscle after ligamentous injury

Brian Noehren[1,2,3,*], **Peter A. Hardy**[4,6], **Anders Andersen**[5,6], **Camille R. Brightwell**[3,7], **Jean L. Fry**[3,7], **Moriel H. Vandsburger**[8], **Katherine L. Thompson**[9], **Christopher S. Fry**[3,7]

[1]Department of Physical Therapy, University of Kentucky

[2]Department of Orthopaedic Surgery & Sports Medicine, University of Kentucky

[3]Center for Muscle Biology, University of Kentucky

[4]Department of Radiology, University of Kentucky

[5]Department of Anatomy & Neurobiology, University of Kentucky

[6]Magnetic Resonance Imaging and Spectroscopy Center, University of Kentucky

[7]Department of Athletic Training and Clinical Nutrition, University of Kentucky

[8]Department of Bioengineering, University of California at Berkeley

[9]Department of Statistics, University of Kentucky

Abstract

Dysregulation and fibrosis of the extracellular matrix (ECM) in skeletal muscle is a consequence of injury. Current ECM assessment necessitates muscle biopsies to evaluate alterations to the muscle ECM, which is often not practical in humans. The goal of this study was to evaluate the potential of a magnetic resonance imaging sequence that quantifies T1ρ relaxation time to predict ECM collagen composition and organization. T1ρ imaging was performed and muscle biopsies obtained from the involved and non-involved vastus lateralis muscle on 27 subjects who had an anterior cruciate ligament (ACL) tear. T1ρ times were quantified via mono exponential decay curve fitted to a series of T1ρ-weighted images. Several ECM indices, including collagen content and organization, were obtained using immunohistochemistry and histochemistry in addition

[*]**Corresponding author**: Brian Noehren, PT, PhD, Department of Physical Therapy, College of Health Sciences, University of Kentucky, 900 S. Limestone, Room 204J, Lexington, KY 40536-0200 (USA).

Author Contributions

BN conducted experiments and data analysis, generated figures, secured funding and drafted the manuscript
AA conducted experiments and assisted with manuscript preparation
PAH conducted experiments and assisted with manuscript preparation
CRB conducted experiments and data analysis and generated figures
JLF conducted experiments and assisted with manuscript revision
MHV conducted data analysis, generated figures and assisted with manuscript preparation
KLT conducted data analysis and assisted with manuscript preparation
CSF conducted experiments and data analysis, generated figures, secured funding and drafted the manuscript
All authors read, edited, and approved of the final manuscript

Competing Interests

None of the authors have any conflict of interest to disclose

to hydroxyproline. Model selection with multiple linear regression was used to evaluate the relationships between T1ρ times and ECM composition. Additionally, the ACL-deficient and healthy limb were compared to determine sensitivity of T1ρ to detect early adaptations in the muscle ECM following injury. We show that T1ρ relaxation time was strongly associated with collagen unfolding (t=4.093, p=0.0007) in the ACL-deficient limb, and collagen 1 abundance in the healthy limb (t=2.75, p=0.014). In addition, we show that T1ρ relaxation time is significantly longer in the injured limb, coinciding with significant differences in several indices of collagen content and remodeling in the ACL-deficient limb. These results support the use of T1ρ to evaluate ECM composition in skeletal muscle in a non-invasive manner.

Keywords

Magnetic Resonance Imaging; Muscle Fibrosis; Extracellular Matrix; T1rho

Introduction:

Skeletal muscle mass and function are critical determinants of health. Compromised muscle function during injury or chronic disease is associated with greater mortality rates and lower quality of life (Ruiz *et al.*, 2008; McLeod *et al.*, 2016; Li *et al.*, 2018). The extracellular matrix (ECM) is intimately involved in the development, growth and repair of muscle and is essential for its function and force transmission (Gillies & Lieber, 2011; Lieber & Ward, 2013). Evaluation of the ECM is increasingly seen as critical given its role in modulating muscle function and adaptation.

The ECM provides structural stability to muscle and represents approximately 5–10 % of total muscle mass in homeostatic conditions (Lieber & Ward, 2013). Expansion of the ECM occurs both when muscle hypertrophies and atrophies. During hypertrophy there is an orderly increase in the ECM, however with atrophy the expansion of the ECM within the perimysium results in a dysregulated environment. The consequence of greater dysregulation is greater distance between muscle fibers and source of nutrients provided by capillaries (Reed & Rubin, 2010), impairment of the resident stem cells to migrate to muscle fibers to initiate a growth or reparative process (Nederveen *et al.*, 2020; Murach *et al.*, 2021), and a decrease in the efficiency by which force is transferred when the muscle contacts (Smith *et al.*, 2011).

Although muscle ECM expansion/fibrosis is a commonly observed pathology, it is often not evaluated in humans given current detection limitations in standard imaging modalities. Analysis of the muscle ECM has required the collection of a muscle biopsy. While extremely informative and powerful, these procedures are not practical to be used in routine clinical practice, are unable to be performed on deep muscles, and are unable to evaluate large areas of the muscle. Imaging modalities such as magnetic resonance imaging (MRI) may hold the key to allow greater ability to assess the ECM in clinical environments. Direct measurement of the ECM with MRI is technically challenging due to extremely short relaxation times of ECM macromolecules, which renders them ostensibly invisible (Sinha *et al.*, 2020). One alternative is to utilize gadolinium-based contrast agents that accumulate

in the extracellular volume between ECM and muscle, and create T1-weighted contrast in proportion to water volume (Carlier *et al.*, 2016). This approach has two drawbacks; namely 1) the indirect assessment of the ECM based on secondary changes in extracellular water volume, and 2) that it poses safety risks due to the use of potentially nephrotoxic gadolinium chelates (Benzon *et al.*, 2021). Rather than perform conventional MR imaging, measurement of T1ρ relaxation time holds promise for imaging of the muscle ECM as a more direct method for assessing macromolecular ECM content. T1ρ imaging has been used for several years to evaluate degradation of cartilage and more recently liver cirrhosis (Regatte *et al.*, 2006; Rauscher *et al.*, 2014). However, validation of the technique against the ECM of muscle remains unreported. Furthermore, to date there have been no studies of the utility of this imaging sequence in muscle to evaluate if it is sensitive to detect changes in the abundance and organization of muscle ECM due to injury. Thus, the purpose of this study is to evaluate the relationship between T1ρ relaxation times and common and clinically meaningful features of the ECM including glycosaminoglycan abundance, total and type 1 collagen abundance, collagen unfolding, and collagen organizational structure. Our second objective was to evaluate the ability to detect differences in the ECM between injured and non-injured limbs in subjects who have had an ACL tear using differences in T1ρ relaxation time. We hypothesized that the injured limb would have a significantly longer T1ρ relaxation time compared to the healthy, intact limb due to increased extracellular volume of water. In addition, we hypothesized that there would be a significant relationship between histomorphological features of the ECM to the T1ρ relaxation time.

Methods:

Ethical Approval

The study was approved by the Institutional Review Board (#42791) at the University of Kentucky, which was performed in accordance with the ethical standards laid down in the 1964 Declaration of Helsinki. This study was registered at ClinicalTrials.gov (ref. no. NCT03364647). Informed written consent was obtained from the patient or parent/legal guardian prior to participation in the study. Additionally, all minors in this study assented to participation.

Research Participants

Twenty seven subjects participated in this study, and subjects' average age was 22.0 (5.2) years with 14 males and 13 females. This data was part of a larger ongoing clinical trial, and the data reported is prior to randomization collected during the subjects' baseline visit. We have previously reported on the study design and inclusion criteria (Erickson *et al.*, 2019), but in brief, to be included subjects must have torn their anterior cruciate ligament (ACL) in the past 10 weeks, be between the ages of 15–40 years old and score an 80/100 on the Cincinnati sports activity scale. Subjects were excluded if they had a previous ACL reconstruction on either limb, had a complete knee dislocation and had any contraindications for either a MRI or muscle biopsy. The MRI and muscle biopsy were performed on the same day in both limbs (ACL-deficient and healthy). The MRI was performed first followed by the muscle biopsy. Both the MRI and the muscle biopsy were of the vastus lateralis muscle, and biopsy collection was aligned with the MRI.

Magnetic Resonance Imaging—Subjects had both their ACL-deficient and healthy limbs imaged on a 3T MAGNETOM Prisma, (Siemens Healthineers, Malvern, PA). A series of localizer scans were used to determine the position and orientation of the superior and inferior extents of the vastus lateralis. A single slice of 10 mm thick and 192 mm × 192 mm was acquired at in line with the placement of the vitamin E tablet. The location was selected from a review of the scout images and by referencing the location of a vitamin E tablet placed on the skin by a trained physiotherapist to coincide with their determination of the center of the vastus lateralis. Images were acquired using an 18-element phased array, flexible, body coil wrapped around the thigh. T1p images were acquired with a spin lock amplitude of 300 Hz, and ten spin lock hold times of (0/10/20/30/40/50/60/70/80/90ms), using a 4 shot, segmented, gradient echo acquisition (TR of 5.8ms, TE 2.5ms, α=10°, BW=560 Hz/pixel, Nex = 2) and shot TR = 1000ms. The spin lock preparation included a B1 and B0-compensated spin lock preparation pulse followed by a chemical shift selective fat saturation pulse (Singh *et al.*, 2014). The sequence employed centric phase encoding to provide exclusive T1rho weighting (Singh *et al.*, 2014). Image data were fit to a mono exponential decay curve (signal vs. spin-lock time) on a pixel-by-pixel basis using custom code employing a non-linear least squares routine in MATLAB (Natick, MA) (Figure 1). Region-of-interest tools in MATLAB were used to outline a region of the vastus lateralis on the calculated maps of T1ρ times consistent with the location of the muscle biopsy.

Quadriceps muscle biopsies—Muscle biopsies from the ACL-deficient and healthy limbs were collected during the same visit for each subject. Subjects were completely weight-bearing at the time of data collection in the current study. Percutaneous muscle biopsies from the vastus lateralis were performed using a Bergström 5 mm muscle biopsy needle with suction (Shanely *et al.*, 2014). Approximately 50 mg was mounted in tragacanth gum on cork and flash frozen in liquid nitrogen-cooled 2-methylbutane. Approximately 20 mg was flash frozen in liquid nitrogen for hydrixyproline analysis. Samples were stored at −80°C until processing.

Hydroxyproline—To estimate total collagen content, hydroxyproline abundance in quadriceps muscle biopsies was measured with a modified protocol using a commercially available Hydroxyproline Assay Kit (MAK008, Millipore Sigma, Darmstadt, Germany), as we have published previously (Brightwell *et al.*, 2020). Briefly, muscle samples were homogenized by bead milling with 0.5-mm zinc oxide beads (Bullet Blender; Next Advance) in ice-cold buffer with phosphatase and protease inhibitor tablets. Following centrifugation, the supernatant was removed, and the pellet containing the collagen fraction was weighed and homogenized in double-distilled water (volume equal to 10x pellet weight; i.e. 100µl double-distilled water for 10mg pellet weight). Following homogenization, the sample was vortexed and a volume of 12M HCl equal to the water was added to hydrolyze the sample overnight at 105°C. The next day after hydrolysis, the sample/hydrolysate was vortexed and 40µl was loaded in duplicate onto a 96-well plate along with hydroxyproline standard included in the Hydroxyproline Assay Kit; samples and standards were dried overnight in an oven at 60°C. Chloramine T/Oxidation Buffer included in the Hydroxyproline Assay Kit was added to each well followed by incubation at room temperature for 5 minutes. Diluted p–dimethylaminobenzaldehyde (DMAB) Reagent was

then added to each well, and the microplate was incubated at 60°C for 90 minutes. Absorbance was measured at 595nm, and hydroxyproline content was calculated using a standard curve and normalized to the loaded sample volume.

Immunohistochemistry—Frozen tissue was sectioned (7 μm) and slides were air dried >1 hr. We have previously published methods for collagen 1 and unfolded collagen with a collagen hybridizing peptide (Abramowitz *et al.*, 2018; Peck *et al.*, 2019). Briefly, slides were fixed in ice cold acetone (−20°C) for 10 minutes, rinsed with PBS and blocked in 1% BSA in PBS for 1 hr at RT. 3Helix-5-FAM conjugate (#F-CHP, 3Helix) was diluted to a working solution (20μM) and placed on a heating block at 80°C for 5 min to denature 3Helix trimers that bind unfolded collagen, then quickly cooled on wet ice for 2 min. Immediately after cooling, anti-collagen 1 (#ab34710, rabbit, 1:200, Abcam, RRID:AB_731684) was added to the 3Helix-PBS solution and slides were incubated overnight at 4°C. The next day, slides were incubated in goat anti-rabbit AF555 (#A21428, Thermofisher) for 1 hr at RT, and then slides were mounted with fluorescent mounting media (#H-1000, Vector Labs).

Picro-sirius red staining to denote total ECM collagen content was performed as previously described (Fry *et al.*, 2017a; Fry *et al.*, 2017b). Sections were fixed in Bouin's solution (#15990-10, Electron Microscopy Sciences) in a water bath at 56°C for 1 h. Following a brief wash, sections were incubated in Sirius Red solution (#ab150681, Abcam; 0.1% in saturated picric acid) for 2 h at room temperature. Slides were then washed in 0.5% acetic acid, dehydrated in 95% and 100% ethanol, equilibrated in xylenes, and mounted in xylene-based mounting media.

Wheat germ agglutinin staining to determine glycosaminoglycan content of the ECM (Emde *et al.*, 2014) was performed as previously described (Fry *et al.*, 2016; Fry *et al.*, 2017a). Briefly, slides were fixed in 4% paraformaldehyde, and incubated overnight AF488-conjugated wheat germ agglutinin (#W11261, ThermoFisher), and then mounted with fluorescent mounting media.

Image Acquisition and Analysis—Images were captured at 10 and 20X magnification at room temperature using a Zeiss upright microscope (AxioImager M1; Zeiss, Oberkochen, Germany). Image analysis was performed in a blinded manner, where the assessor did not know if the image was from the injured or healthy limb. Analyses were carried our using Image J Fiji or Zeiss Zen software (v3.1).

Collagen 1, wheat germ agglutinin and unfolded collagen images were quantified to measure expansion of key components and remodeling of the muscle ECM using the thresholding feature of Zeiss Zen, and the area occupied by collagen 1, wheat germ agglutinin and unfolded collagen were independently expressed as a percentage relative to the total muscle area (mm^2). Picro-sirius red staining was quantified to measure total collagen content of the muscle ECM using Image J Fiji software as previously described (Fry *et al.*, 2017a). The area of picro-sirius red+ collagen was normalized to the total muscle area (mm^2). To evaluate collagen packing density, picro-sirius red-stained muscle sections were also viewed under circularly polarized light (Smith & Barton, 2014). Under quarter wavelength polarized

light, whole muscle images were obtained as with light microscopy to quantify densely packed (red) and loosely packed (green) collagen using the ImageJ FIJI Color Pixel Counter and expressed relative to total muscle area and to the area of total collagen/pirco-sirius red (Junqueira *et al.*, 1979; Lattouf *et al.*, 2014).

Statistical Analyses—To begin, data were plotted to check distributions of independent and dependent variables. Prior to data analysis, picro-sirius red collagen and polarized light measures (densely packed [red] and loosely packed [green] collagen) were log-transformed using a natural logarithm due to skewness. Data are presented as mean ± standard deviation with individual data points overlaid on all graphs. Next, separate multiple linear regression models were built for ACL-deficient and healthy limbs in order to identify predictors of T1ρ times using statistical model selection methods. Since observations from non-injured and injured limbs within the same subjects are dependent, inference from a single traditional multiple linear regression analysis for both limbs would be invalid for this data. In addition, we were not interested in comparing limbs, so the ACL-deficient and healthy limbs were analyzed separately. In this analysis, statistical model selection was performed through an exhaustive search (used to identify combinations of potential explanatory variables related to T1ρ relaxation time as the response variable) (Neter *et al.*, 1996). In this case, all possible models with 3 or fewer explanatory variables were fit using T1ρ relaxation time as an outcome. Candidate models were compared using all available data for the variables under consideration. Two model selection criteria (R^2 and adjusted R^2) were used in order to identify candidate models for further consideration.

After candidate models were identified, we chose a single biologically-informed multiple linear regression model for each of the ACL-deficient and healthy limbs for further exploration. Tables 1 and 2 show the R^2 and adjusted R^2 values from models with at most three explanatory variables for both the ACL-deficient (Table 1) and healthy (Table 2) limbs for all available data. For each number of explanatory variables, only the top five models are reported if more than five potential models exist. Residual plots were checked for violations of model assumptions in the candidate models. Individual t-tests for predictor variables are reported based on the final multiple linear regression models. Next, paired t-tests were performed to identify any differences in mean T1ρ time and predictors between ACL-deficient and healthy limbs. All analyses were performed in R version 3.6.1 and model selection was performed using the package leaps (Neter *et al.*, 1996).

Results:

T1ρ relaxation time and markers of collagen unfolding and content are elevated in the ACL-deficient limb

T1ρ relaxation time in ACL-deficient (Figure 2, top row) and corresponding healthy (Figure 2, bottom row) limbs for individuals with low (left), medium (middle), and high (right) severity of injury reveal meaningful differences in T1ρ relaxation time in the vastus lateralis muscle (faint red arrow denoting vastus lateralis) as a function of injury. T1ρ relaxation time was statistically different and longer in the ACL-deficient limb (Figure 3, p=0.003),

supporting the use of T1ρ as a sensitive imaging modality to evaluate changes in the ECM composition in skeletal muscle following ligamentous injury.

To verify that the ACL-deficient limb showed alterations in the muscle ECM, we utilized a number of indices associated with collagen content, organization and other key components of the ECM. Hydroxyproline abundance was elevated ~46% in the ACL-deficient limb ($p<0.0001$, Figure 4A). As we have published previously (Noehren *et al.*, 2016; Fry *et al.*, 2017a; Peck *et al.*, 2019), the ACL-deficient limb displayed elevated abundance of total collagen ($p=0.003$), collagen 1 ($p<0.0001$), unfolded collagen ($p<0.0001$) and loosely organized collagen ($p=0.026$, Figure 4, representative images in Figure 5), indicating early remodeling of the ECM following injury in skeletal muscle. Densely packed collagen ($p=0.297$) and wheat germ agglutinin ($p=0.542$) were not statistically different between limbs (Figure 4). Divergence in the differences between limbs among biopsy outcome variables may provide temporal information on early indicators of ECM remodeling and pathology given the acute time frame the biopsies were collected following ACL injury (25.3 [15.8] days post-injury).

Variance in on-resonance T1ρ relaxation with skeletal muscle collagen content and organization

Within the ACL-deficient limb, the final multiple linear regression model selected explained 49% of the variation in T1ρ relaxation time by including unfolded collagen, hydroxyproline, and wheat germ agglutinin (Figure 6). We note that the overall F-test is also significant ($p=0.006$), indicating that at least one of the three predictor variables is helpful in predicting T1ρ relaxation time. Indeed, T1ρ relaxation time was strongly associated with unfolded collagen ($t=4.093$, $p=0.0007$) in the ACL-deficient limb. In addition, by holding certain predictors in the model fixed, we were then able to evaluate how other predictors change or effect T1ρ relaxation time. This allows us to provide an estimate of the effect unfolded collagen would have on T1ρ relaxation time. Specifically, when we hold hydroxyproline and wheat germ agglutinin fixed, we estimate that T1ρ relaxation time increases 45ms for each additional percent increase in unfolded collagen.

Within the healthy limb, the final multiple linear regression model explains 38% of the variation in T1ρ relaxation time (Figure 7) with the inclusion of three predictors: total collagen, collagen type 1 and hydroxyproline. We note that the overall F-test is also significant ($p=0.0394$), indicating that at least one of these predictor variables is helpful in predicting T1ρ relaxation time in the healthy limb. Specifically, T1ρ relaxation time was strongly associated with collagen 1 ($t=2.747$, $p=0.014$) and total collagen ($t=-2.216$, $p=0.041$) in the healthy limb quadriceps. We choose to focus on collagen 1 as it is the primary fibular collagen isoform found in skeletal muscle (Järvinen *et al.*, 2002). To evaluate the effect of greater fibular collagen (type I collagen) on T1ρ relaxation time, we estimated that by holding total collagen content and hydroxyproline fixed, T1ρ relaxation time increases by 45ms for each additional percent increase in collagen 1. In addition, to evaluate the effect of hydroxyproline on T1ρ relaxation time, we estimated that by holding type 1 collagen and total content fixed, T1ρ relaxation time increases by 0.95 ms for each μg/μl increase in hydroxyproline content.

Discussion:

Our findings demonstrate a relationship between altered T1ρ relaxation time in the vastus lateralis muscle that we relate to the abundance and organization of key components of its ECM. In the ACL-deficient limb we observed elevated abundance of total collagen and increased indices of unfolded collagen that were associated with longer T1ρ relaxation times. In the healthy, contralateral limb, measures of total collagen abundance explained a greater degree of the variance in T1ρ relaxation times. Importantly, we observed that changes in T1ρ times were sensitive to differences between the ACL deficient and healthy limb congruent with results from our cellular phenotyping. Collectively, these data provide evidence for a relationship between adaptations to the muscle ECM and T1ρ times measured noninvasively at 3T.

Previously we have reported alterations to the muscle ECM following ACL injury including elevated abundance of collagen (Noehren *et al.*, 2016; Fry *et al.*, 2017a; Peck *et al.*, 2019). The excessive accumulation of ECM components, particularly collagen, can result in permanent scar formation, which can affect muscle function (Abramowitz *et al.*, 2018; Brashear *et al.*, 2020). The identification of non-invasive imaging techniques that are congruent and orthogonal to more traditional histomorphology and cellular phenotyping approaches to assess the muscle ECM offers clinical benefit. Our principle finding was the significant relationship between T1ρ relaxation times and collagen unfolding, hydroxyproline and glycosaminoglycan content of the ECM within the vastus lateralis muscle of the ACL deficient limb. The affinity of collagen and water is highly impacted by collagen organization (McGee *et al.*, 2012; Gonzalez & Wess, 2013), and may provide the link between collagen remodeling and density and T1ρ relaxation times measured by MRI. Longer T1ρ relaxation times in other tissues such as cartilage and the liver have been attributed to greater extracellular water content and thus a higher fraction of each voxel with long T1ρ times of water (Regatte *et al.*, 2006; Rauscher *et al.*, 2014). Increased tension at interfaces formed as collagen unfolds generates local gradients in the ECM that accelerate water transfer, promoting the diffusion of water within the ECM (McGee *et al.*, 2012). Our data show that a greater degree of collagen unfolding within the ECM correlates with longer T1ρ relaxation times. The collagen hybridizing peptide we employ specifically hybridizes to unfolded collagen chains as an index of collagen remodeling activity in various tissues (Hwang *et al.*, 2017), including skeletal muscle (Abramowitz *et al.*, 2018; Peck *et al.*, 2019; Brightwell *et al.*, 2020). In other tissues such as articular cartilage, greater dispersion/reduced density of collagen results in a longer T1ρ relaxation time (Collins *et al.*, 2019). Disruption of collagen triple helices enhances the water content of the ECM and reduces dipole interactions between bound water molecules, cumulatively leading to a lengthening of the relaxation time as seen during tendonopathy (Kijowski *et al.*, 2017; Sharafi *et al.*, 2017b). In this state, unbound water diffuses throughout the ECM, manifested by longer relaxation times. Additionally, glycosaminoglycan content of the muscle ECM was also associated in our model with longer T1ρ relaxation times. These results were somewhat expected given prior work quantifying glycosaminoglycan levels in muscle ECM using T1ρ (Menon *et al.*, 2019). T1ρ is sensitive to interactions related to the chemical exchange between interstitial water and macromolecules present in the ECM,

such as glycosaminoglycans (Mlynárik *et al.*, 2004). In particular, the glycosaminoglycan hyaluronic acid is highly hydrophilic and abundant within the ECM (Calve *et al.*, 2012), orchestrating water molecule interaction(s) via its hydroxyl (-OH) groups during MRI mapping (Ponsiglione *et al.*, 2020). Glycosaminoglycan content is elevated in fibrotic muscle pathologies through direct biopsy analysis (Negroni *et al.*, 2014). Our data support the use of T1ρ as a noninvasive marker of overall ECM dysregulation and remodeling that occurs within skeletal muscle following ligamentous injury.

Interestingly, we found that within the healthy contralateral limb measures of collagen abundance explained the greatest variance in T1ρ relaxation time. Collagen 1 content, the most abundant collagen isoform within skeletal muscle (Järvinen *et al.*, 2002), was associated with longer T1ρ relaxation time in the healthy limb, along with total collagen abundance as assessed through picro-sirius red histomorphometry and hydroxyproline. Hydroxyproline is a modified amino acid that is abundant in collagen and serves as a direct measure of the amount of collagen present. Hierarchical modeling revealed different effectors between the ACL deficient and healthy limb, further supporting the premise that T1ρ relaxation time is a sensitive marker of ECM dysregulation within skeletal muscle. The muscle ECM components that were most strongly related to T1ρ relaxation in the healthy limb are reflective of a more stable collagen interstitial environment and hence a shorter T1ρ relaxation time. T1ρ relaxation time is significantly longer in the ACL-injured limb. The ability to establish between limb differences after modest adaptations within the quadriceps ECM in the same participant shows T1ρ to be a sensitive marker of ECM remodeling and dysregulation.

Monitoring T1ρ relaxation time as a noninvasive biomarker of muscle ECM remodeling may provide valuable information on disease progression, even when of a subclinical nature. Our findings show collagen deposition and ECM dysregulation in the ACL deficient limb occur relatively quickly following ACL rupture, more rapidly than we have previously reported (Noehren *et al.*, 2016; Fry *et al.*, 2017a; Peck *et al.*, 2019). Acute injuries (Brightwell *et al.*, 2020; Lee *et al.*, 2020), chronic illness (Abramowitz *et al.*, 2018), aging (Brack *et al.*, 2007) and dystrophies (Mann *et al.*, 2011; Lieber & Ward, 2013) all show dysregulation of the muscle ECM that contributes to disease pathophysiology. We report significant differences in T1ρ relaxation time in the ACL-deficient quadriceps that were associated with alterations in the collagen fiber network and changes in macromolecular content of the quadriceps ECM. The ACL deficient limb showed remodeling and deposition of collagen, but the degree of collagen accumulation is of far less severity than that associated with muscular dystrophies (Mann *et al.*, 2011; Lieber & Ward, 2013). Hence, our findings highlight the sensitivity of T1ρ imaging to quantitatively identify early and sub-clinical indicators of muscle ECM dysregulation (Rybak & Torriani, 2003). Non-invasive imaging has promise both for diagnosing and for quantitatively tracking muscle tissue damage and disease/injury progression.

This study is not without limitations. As the focus of this work was on a clinical application to assess *in vivo* clinical conditions we did not perform evaluations of T1ρ against phantoms with known percentages of collagen content. Further, due to the challenges of securing muscle biopsies we were only able to evaluate the relationship between T1ρ relaxation

time within the vastus lateralis muscle. Additionally, given size constraints of obtained human biopsies, we were unable to segregate hierarchical organization of the ECM (e.g. perimysium/endomysium) to further explain variance in T1ρ relaxation time. In Figure 1 the deviations of the data from the mono-exponential model could be evidence of a bi- or multi-exponential decay. This behavior may reflect the heterogeneity of the environment in the muscle. As we recorded only 10 echoes and, considering the known difficulty of fitting multiple exponential functions to a small number of data points, we did not evaluate this observation further. Preliminary reports in other populations point to the potential of this approach that should be explored in future work(Sharafi *et al.*, 2017a). Lastly, we were not able to consider evaluating other sequences such as T2 mapping that may add additional information regarding muscle function. Having established T1ρ as a marker of ECM/collagen dysregulation, future studies should consider leveraging multiple imaging sequences.

The results of this experiment identify T1ρ as a non-invasive marker of collagen dysregulation within skeletal muscle ECM. Furthermore, T1ρ relaxation time was sensitive to detect modest differences in collagen deposition and remodeling between ACL-deficient and healthy, contralateral limbs. Evaluation of changes in collagen content and organization and other macromolecular components within skeletal muscle is critical for the evaluation of patients with a variety of conditions and to assess the effect of interventions to improve muscle quality. These results offer a potential clinical tool to evaluate muscle ECM pathophysiology, which until now exclusively required a muscle biopsy, limiting feasibility.

Supplementary Material

Refer to Web version on PubMed Central for supplementary material.

Acknowledgements

The authors would like to thank the subjects for their participation. We would also like to thank Madison Grzesiak and Madalyn Romines for their assistance with data processing.

Funding

Research reported in this publication was supported by the National Institute of Arthritis and Musculoskeletal and Skin Diseases of the National Institutes of Health under Award Numbers R01 AR071398, R01 AR072061 and R01 AR071398-04S1, as well as by the National Institute of Biomedical Imaging and Bioengineering of the National Institutes of Health under award Number P41EB015893, and the National Institutes of Health National Center for Advancing Translational Sciences through award number UL1TR001998. The content is solely the responsibility of the authors and does not necessarily represent the official views of the National Institutes of Health.

Data Availability Statement

The data that support the findings of this study are available within the paper and the Supplementary Statistical Summary Document. Additional data are available from the corresponding author upon reasonable request.

References:

Abramowitz MK, Paredes W, Zhang K, Brightwell CR, Newsom JN, Kwon H, Custodio M, Buttar RS, Farooq H, Zaidi B, Pai R, Pessin JE, Hawkins M & Fry CS. (2018). Skeletal muscle fibrosis

is associated with decreased muscle inflammation and weakness in patients with chronic kidney disease. Am J Physiol Renal Physiol.

Benzon HT, Maus TP, Kang HR, Provenzano DA, Bhatia A, Diehn F, Nelson A, McCormick ZL, Liu BP, de Andres Ares J, Anitescu M, Blackham K, Bhaskar A, Brill S, Collins J, Gulve A, Hurley RW, Jeon YH, Moon JY, Rauck RL, Rodes M, Lee RK, Shah V, Shanthanna H, van Zundert J, Huntoon M, Rathmell JP, Borges MS, Cohen SP & Greenberger PA. (2021). The Use of Contrast Agents in Interventional Pain Procedures: A Multispecialty and Multisociety Practice Advisory on Nephrogenic Systemic Fibrosis, Gadolinium Deposition in the Brain, Encephalopathy After Unintentional Intrathecal Gadolinium Injection, and Hypersensitivity Reactions. Anesth Analg.

Brack AS, Conboy MJ, Roy S, Lee M, Kuo CJ, Keller C & Rando TA. (2007). Increased Wnt signaling during aging alters muscle stem cell fate and increases fibrosis. Science 317, 807–810. [PubMed: 17690295]

Brashear SE, Wohlgemuth RP, Gonzalez G & Smith LR. (2020). Passive stiffness of fibrotic skeletal muscle in mdx mice relates to collagen architecture. J Physiol.

Brightwell CR, Hanson ME, El Ayadi A, Prasai A, Wang Y, Finnerty CC & Fry CS. (2020). Thermal injury initiates pervasive fibrogenesis in skeletal muscle. Am J Physiol Cell Physiol.

Calve S, Isaac J, Gumucio JP & Mendias CL. (2012). Hyaluronic acid, HAS1, and HAS2 are significantly upregulated during muscle hypertrophy. Am J Physiol Cell Physiol 303, C577–588. [PubMed: 22785117]

Carlier PG, Marty B, Scheidegger O, Loureiro de Sousa P, Baudin PY, Snezhko E & Vlodavets D. (2016). Skeletal Muscle Quantitative Nuclear Magnetic Resonance Imaging and Spectroscopy as an Outcome Measure for Clinical Trials. J Neuromuscul Dis 3, 1–28. [PubMed: 27854210]

Collins AT, Hatcher CC, Kim SY, Ziemian SN, Spritzer CE, Guilak F, DeFrate LE & McNulty AL. (2019). Selective Enzymatic Digestion of Proteoglycans and Collagens Alters Cartilage T1rho and T2 Relaxation Times. Ann Biomed Eng 47, 190–201. [PubMed: 30288634]

Emde B, Heinen A, Gödecke A & Bottermann K. (2014). Wheat germ agglutinin staining as a suitable method for detection and quantification of fibrosis in cardiac tissue after myocardial infarction. European journal of histochemistry : EJH 58, 2448. [PubMed: 25578975]

Erickson LN, Lucas KCH, Davis KA, Jacobs CA, Thompson KL, Hardy PA, Andersen AH, Fry CS & Noehren BW. (2019). Effect of Blood Flow Restriction Training on Quadriceps Muscle Strength, Morphology, Physiology, and Knee Biomechanics Before and After Anterior Cruciate Ligament Reconstruction: Protocol for a Randomized Clinical Trial. Phys Ther.

Fry CS, Johnson DL, Ireland ML & Noehren B. (2017a). ACL injury reduces satellite cell abundance and promotes fibrogenic cell expansion within skeletal muscle. J Orthop Res 35, 1876–1885. [PubMed: 27935172]

Fry CS, Kirby TJ, Kosmac K, McCarthy JJ & Peterson CA. (2017b). Myogenic Progenitor Cells Control Extracellular Matrix Production by Fibroblasts during Skeletal Muscle Hypertrophy. Cell Stem Cell 20, 56–69. [PubMed: 27840022]

Fry CS, Porter C, Sidossis LS, Nieten C, Reidy PT, Hundeshagen G, Mlcak R, Ramussen BB, Lee JO, Suman OE, Herndon DN & Finnerty CC. (2016). Satellite cell activation and apoptosis in skeletal muscle from severely burned children. The Journal of physiology.

Gillies AR & Lieber RL. (2011). Structure and function of the skeletal muscle extracellular matrix. Muscle Nerve 44, 318–331. [PubMed: 21949456]

Gonzalez LG & Wess TJ. (2013). The effects of hydration on the collagen and gelatine phases within parchment artefacts. Heritage Science 1, 14.

Hwang J, Huang Y, Burwell TJ, Peterson NC, Connor J, Weiss SJ, Yu SM & Li Y. (2017). In Situ Imaging of Tissue Remodeling with Collagen Hybridizing Peptides. ACS Nano 11, 9825–9835. [PubMed: 28877431]

Järvinen TA, Józsa L, Kannus P, Järvinen TL & Järvinen M. (2002). Organization and distribution of intramuscular connective tissue in normal and immobilized skeletal muscles. An immunohistochemical, polarization and scanning electron microscopic study. J Muscle Res Cell Motil 23, 245–254. [PubMed: 12500904]

Junqueira LC, Bignolas G & Brentani RR. (1979). Picrosirius staining plus polarization microscopy, a specific method for collagen detection in tissue sections. Histochem J 11, 447–455. [PubMed: 91593]

Kijowski R, Wilson JJ & Liu F. (2017). Bicomponent ultrashort echo time T2* analysis for assessment of patients with patellar tendinopathy. J Magn Reson Imaging 46, 1441–1447. [PubMed: 28263448]

Lattouf R, Younes R, Lutomski D, Naaman N, Godeau G, Senni K & Changotade S. (2014). Picrosirius red staining: a useful tool to appraise collagen networks in normal and pathological tissues. The journal of histochemistry and cytochemistry : official journal of the Histochemistry Society 62, 751–758. [PubMed: 25023614]

Lee C, Liu M, Agha O, Kim HT, Feeley BT & Liu X. (2020). Beige FAPs Transplantation Improves Muscle Quality and Shoulder Function After Massive Rotator Cuff Tears. Journal of orthopaedic research : official publication of the Orthopaedic Research Society 38, 1159–1166. [PubMed: 31808573]

Li R, Xia J, Zhang XI, Gathirua-Mwangi WG, Guo J, Li Y, McKenzie S & Song Y. (2018). Associations of Muscle Mass and Strength with All-Cause Mortality among US Older Adults. Med Sci Sports Exerc 50, 458–467. [PubMed: 28991040]

Lieber RL & Ward SR. (2013). Cellular mechanisms of tissue fibrosis. 4. Structural and functional consequences of skeletal muscle fibrosis. Am J Physiol Cell Physiol 305, C241–252. [PubMed: 23761627]

Mann CJ, Perdiguero E, Kharraz Y, Aguilar S, Pessina P, Serrano AL & Munoz-Canoves P. (2011). Aberrant repair and fibrosis development in skeletal muscle. Skelet Muscle 1, 21. [PubMed: 21798099]

McGee MP, Morykwas M, Shelton J & Argenta L. (2012). Collagen unfolding accelerates water influx, determining hydration in the interstitial matrix. Biophys J 103, 2157–2166. [PubMed: 23200049]

McLeod M, Breen L, Hamilton DL & Philp A. (2016). Live strong and prosper: the importance of skeletal muscle strength for healthy ageing. Biogerontology 17, 497–510. [PubMed: 26791164]

Menon RG, Raghavan P & Regatte RR. (2019). Quantifying muscle glycosaminoglycan levels in patients with post-stroke muscle stiffness using T. Sci Rep 9, 14513. [PubMed: 31601831]

Mlynárik V, Szomolányi P, Toffanin R, Vittur F & Trattnig S. (2004). Transverse relaxation mechanisms in articular cartilage. J Magn Reson 169, 300–307. [PubMed: 15261626]

Murach KA, Peck BD, Policastro RA, Vechetti IJ, Van Pelt DW, Dungan CM, Denes LT, Fu X, Brightwell CR, Zentner GE, Dupont-Versteegden EE, Richards CI, Smith JJ, Fry CS, McCarthy JJ & Peterson CA. (2021). Early Satellite Cell Communication Creates a Permissive Environment for Long-Term Muscle Growth. iScience, 102372. [PubMed: 33948557]

Nederveen JP, Joanisse S, Thomas ACQ, Snijders T, Manta K, Bell KE, Phillips SM, Kumbhare D & Parise G. (2020). Age-related changes to the satellite cell niche are associated with reduced activation following exercise. FASEB J 34, 8975–8989. [PubMed: 32463134]

Negroni E, Henault E, Chevalier F, Gilbert-Sirieix M, Van Kuppevelt TH, Papy-Garcia D, Uzan G & Albanese P. (2014). Glycosaminoglycan modifications in Duchenne muscular dystrophy: specific remodeling of chondroitin sulfate/dermatan sulfate. J Neuropathol Exp Neurol 73, 789–797. [PubMed: 25003237]

Neter J, Kutner MH, Nachtsheim CJ & Wasserman W. (1996). Applied linear statistical models. McGraw-Hill/Irwin.

Noehren B, Andersen A, Hardy P, Johnson DL, Ireland ML, Thompson KL & Damon B. (2016). Cellular and Morphological Alterations in the Vastus Lateralis Muscle as the Result of ACL Injury and Reconstruction. The Journal of bone and joint surgery American volume 98, 1541–1547. [PubMed: 27655981]

Peck BD, Brightwell CR, Johnson DL, Ireland ML, Noehren B & Fry CS. (2019). Anterior Cruciate Ligament Tear Promotes Skeletal Muscle Myostatin Expression, Fibrogenic Cell Expansion, and a Decline in Muscle Quality. Am J Sports Med 47, 1385–1395. [PubMed: 30995070]

Ponsiglione AM, Russo M & Torino E. (2020). Glycosaminoglycans and Contrast Agents: The Role of Hyaluronic Acid as MRI Contrast Enhancer. Biomolecules 10.

Rauscher I, Eiber M, Ganter C, Martirosian P, Safi W, Umgelter A, Rummeny EJ & Holzapfel K. (2014). Evaluation of T1rho as a potential MR biomarker for liver cirrhosis: comparison of healthy control subjects and patients with liver cirrhosis. European journal of radiology 83, 900–904. [PubMed: 24661616]

Reed RK & Rubin K. (2010). Transcapillary exchange: role and importance of the interstitial fluid pressure and the extracellular matrix. Cardiovasc Res 87, 211–217. [PubMed: 20472565]

Regatte RR, Akella SVS, Lonner JH, Kneeland JB & Reddy R. (2006). T1ρ relaxation mapping in human osteoarthritis (OA) cartilage: Comparison of T1ρ with T2. Journal of Magnetic Resonance Imaging 23, 547–553. [PubMed: 16523468]

Ruiz JR, Sui X, Lobelo F, Morrow JR, Jackson AW, Sjostrom M & Blair SN. (2008). Association between muscular strength and mortality in men: prospective cohort study. British Medical Journal 337.

Rybak LD & Torriani M. (2003). Magnetic resonance imaging of sports-related muscle injuries. Top Magn Reson Imaging 14, 209–219. [PubMed: 12777891]

Shanely RA, Zwetsloot KA, Triplett NT, Meaney MP, Farris GE & Nieman DC. (2014). Human skeletal muscle biopsy procedures using the modified Bergstrom technique. J Vis Exp, 51812. [PubMed: 25285722]

Sharafi A, Chang G & Regatte RR. (2017a). Bi-component T1rho and T2 Relaxation Mapping of Skeletal Muscle In-Vivo. Sci Rep 7, 14115. [PubMed: 29074883]

Sharafi A, Chang G & Regatte RR. (2017b). Bi-component T1ρ and T2 Relaxation Mapping of Skeletal Muscle In-Vivo. Sci Rep 7, 14115. [PubMed: 29074883]

Singh A, Haris M, Cai K, Kogan F, Hariharan H & Reddy R. (2014). High resolution T1ρ mapping of in vivo human knee cartilage at 7T. PLoS One 9, e97486. [PubMed: 24830386]

Sinha U, Malis V, Chen JS, Csapo R, Kinugasa R, Narici MV & Sinha S. (2020). Role of the Extracellular Matrix in Loss of Muscle Force With Age and Unloading Using Magnetic Resonance Imaging, Biochemical Analysis, and Computational Models. Front Physiol 11, 626. [PubMed: 32625114]

Smith LR & Barton ER. (2014). Collagen content does not alter the passive mechanical properties of fibrotic skeletal muscle in mdx mice. Am J Physiol Cell Physiol 306, C889–898. [PubMed: 24598364]

Smith LR, Lee KS, Ward SR, Chambers HG & Lieber RL. (2011). Hamstring contractures in children with spastic cerebral palsy result from a stiffer extracellular matrix and increased in vivo sarcomere length. The Journal of physiology 589, 2625–2639. [PubMed: 21486759]

Key Points:

- Dysregulation and fibrotic transformation of the skeletal muscle extracellular matrix (ECM) is a common pathology associated with injury and aging
- Studies of the muscle ECM in humans have necessitated the use of biopsies, which are impractical in many settings
- Non-invasive MRI T1ρ relaxation time was validated to predict ECM collagen composition and organization with aligned T1ρ imaging and biopsies of the vastus lateralis in the heathy limb and Anterior Cruciate Ligament (ACL)-deficient limb of 27 subjects
- T1ρ relaxation time was strongly associated with collagen abundance and unfolding in the ACL deficient limb, and T1ρ relaxation time was strongly associated with total collagen abundance in the healthy limb
- T1ρ relaxation time was significantly longer in the ACL deficient limb, coinciding with significant increases in several indices of muscle collagen content and remodeling supporting the use of T1ρ to non-invasively evaluate ECM composition and pathology in skeletal muscle

Authors' Translational Perspective

The extracellular matrix (ECM) is intimately involved in the development, growth and repair of skeletal muscle and is essential for its function and force transmission. Evaluation of the ECM is increasingly seen as critical given its role in modulating muscle function and adaptation. Historically, studies of the muscle ECM in humans have necessitated the use of biopsies, which are impractical in many settings. In the current study, we sought to validate non-invasive MRI T1ρ relaxation time to predict muscle ECM collagen composition and organization. We obtained aligned T1ρ images and biopsies of the vastus lateralis in a cohort of human subjects who have undergone an injury to their Anterior Cruciate Ligament (ACL). Images and biopsies were collected from both the ACL-deficient and healthy limb. We hypothesized that the ACL-deficient limb would have a significantly longer T1ρ relaxation time compared to the healthy, intact limb due to increased extracellular volume of water. In addition, we hypothesized that there would be a significant relationship between histomorphological features of the ECM to the T1ρ relaxation time. We found that T1ρ relaxation time was strongly associated with collagen unfolding and organization in the ACL-deficient limb, and T1ρ relaxation time was strongly associated with total collagen abundance in the healthy limb. T1ρ relaxation time was significantly longer in the ACL deficient limb, coinciding with significant increases in several indices of muscle collagen content and remodeling supporting the use of T1ρ to non-invasively evaluate ECM composition and pathology in human skeletal muscle.

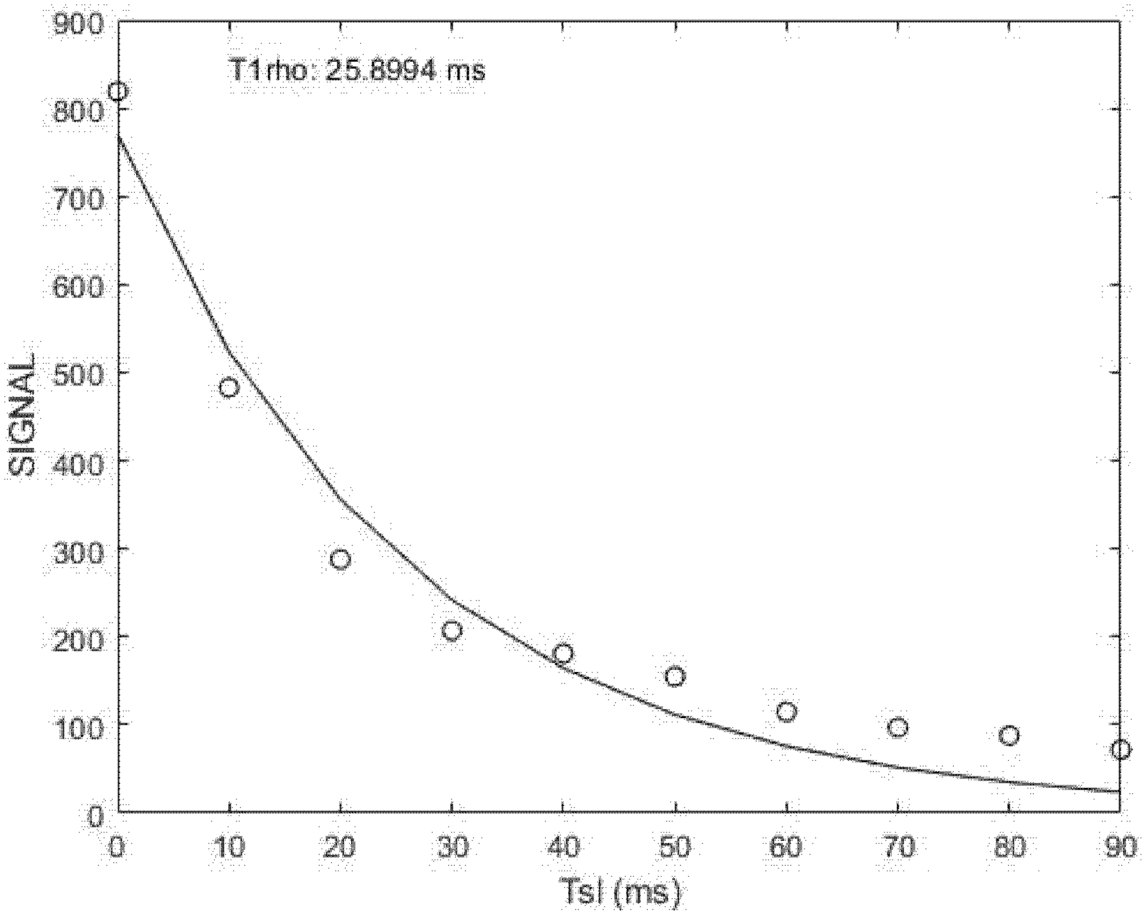

Figure 1. Example of T1ρ image data fit to a mono exponential decay curve (signal vs. spin-lock time). Image intensity data from raw T1rho images were taken from a single pixel located in the VL in one subject.

The uncertainty in the data points was estimated as the standard deviation of the pixels in the background of the raw T1ρ images, which varied only slightly from echo-to-echo, and had an amplitude smaller than the size of the symbols. The data was fit, using a non-linear, least squares algorithm, to a mono-exponential decay model from which we derived the amplitude and the decay rate for the model.

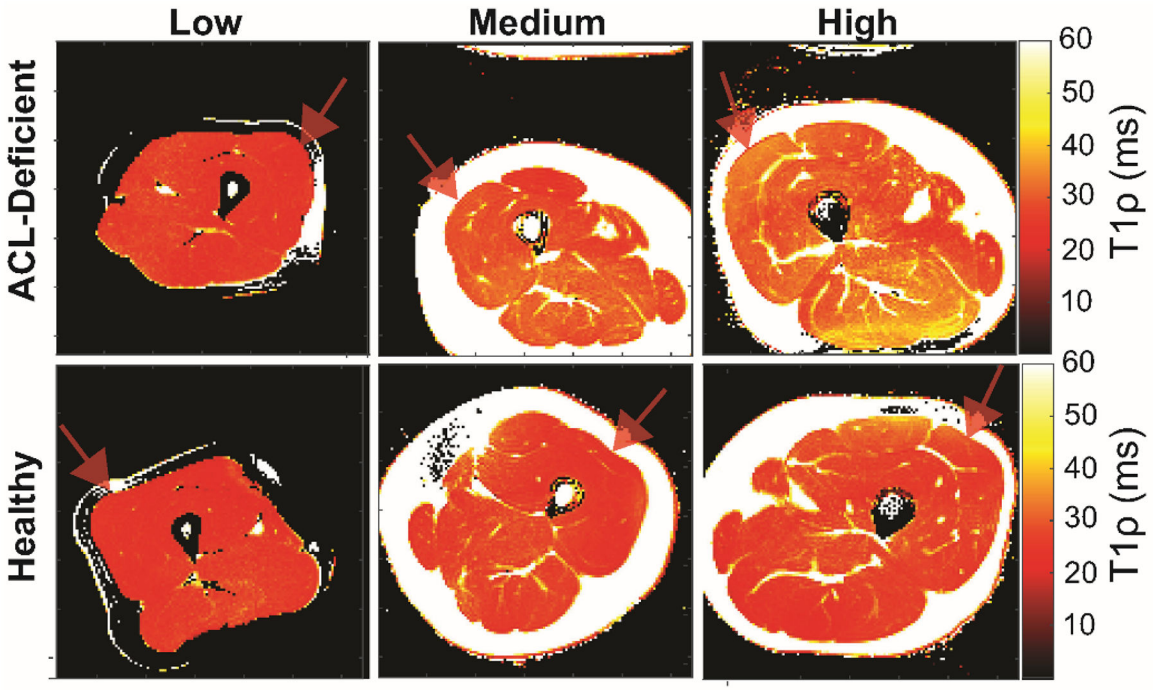

Figure 2. Maps of T1ρ times in patients with increasing magnitude enables quantitative visualization of muscle tissue alterations.

The maps of T1ρ times in ACL-deficient (top row) and corresponding uninjured healthy (bottom row) limbs for individuals with low (left), medium (middle), and high (right) T1ρ times reveal meaningful differences can be visualized in the vastus lateralis muscle (faint red arrow) as a function of alterations within the muscle. Mean T1ρ times in the representative examples shown were: Low (24.6ms [ACL-deficient] vs. 24.2ms [Healthy]); Medium (31.1ms [ACL-deficient] vs. 26.9ms [Healthy]); High: (34.6ms [ACL-deficient] vs. 30.4ms [Healthy]). Elevated T1ρ times result from increased extracellular water volume secondary to enhanced extracellular matrix formation.

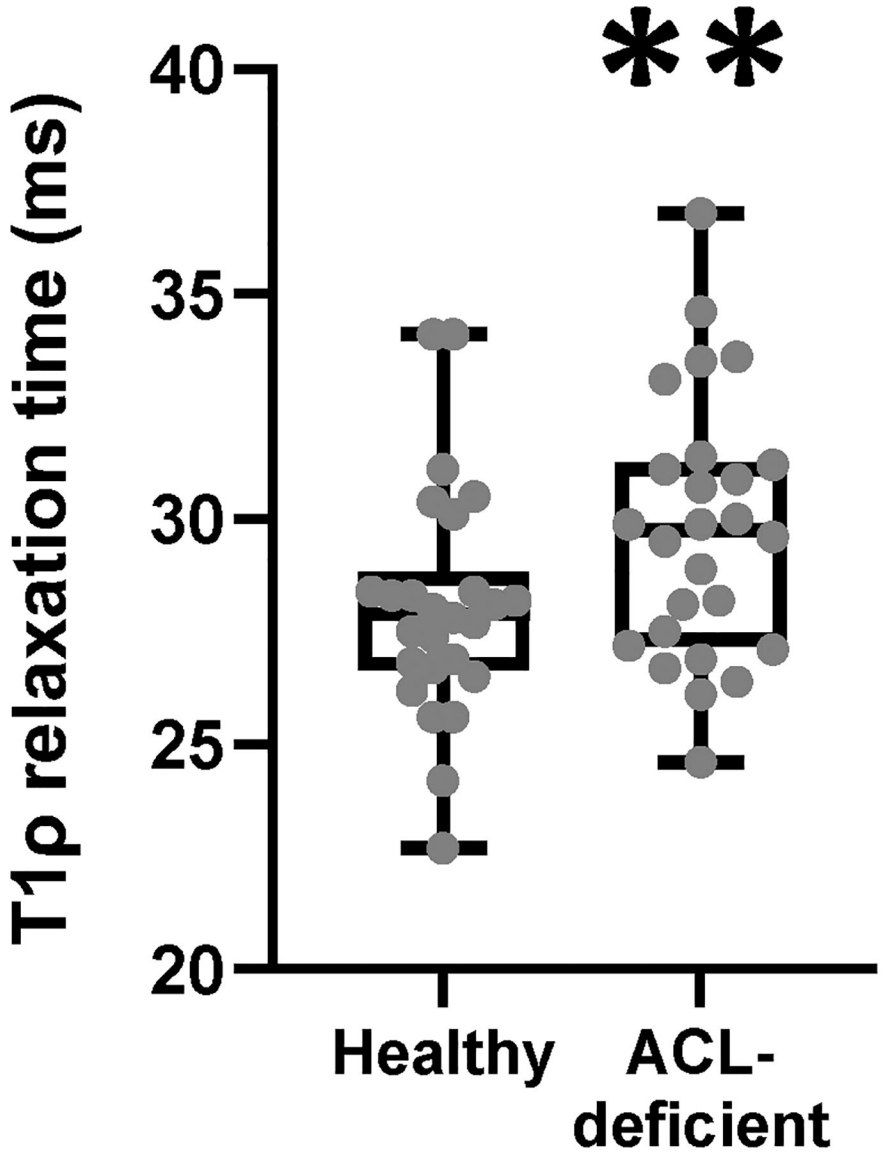

Figure 3. T1ρ relaxation time is longer in ACL-deficient quadriceps.

N=27 participants who underwent bilateral T1ρ imaging. Data are compared with a paired student's t-test. ** denotes $p<0.01$.

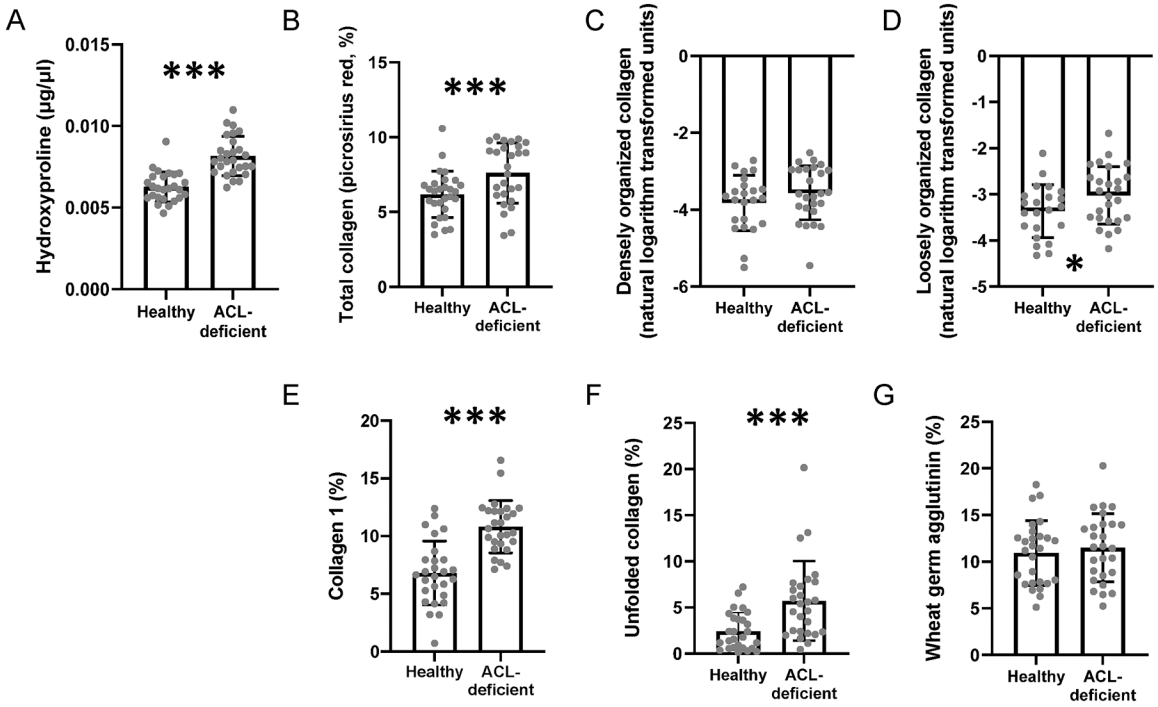

Figure 4. Collagen unfolding, organization and total content are elevated in ACL-deficient quadriceps muscle.

(A) Quantification of hydroxyproline in the healthy and ACL-deficient quadriceps; (B) Quantification of total collagen in the healthy and ACL-deficient quadriceps; (C) Quantification of densely organized collagen in the healthy and ACL-deficient quadriceps; (D) Quantification of loosely organized collagen in the healthy and ACL-deficient quadriceps; (E) Quantification of collagen 1 in the healthy and ACL-deficient quadriceps (F) Quantification of unfolded collagen in the healthy and ACL-deficient quadriceps; (G) Quantification of glycosaminoglycan content in the healthy and ACL-deficient quadriceps. N=27 participants who underwent bilateral vastus lateralis biopsies. Data are compared with a paired student's t-test. * denotes $p<0.05$, ** denotes $p<0.01$, *** denotes $p<0.001$.

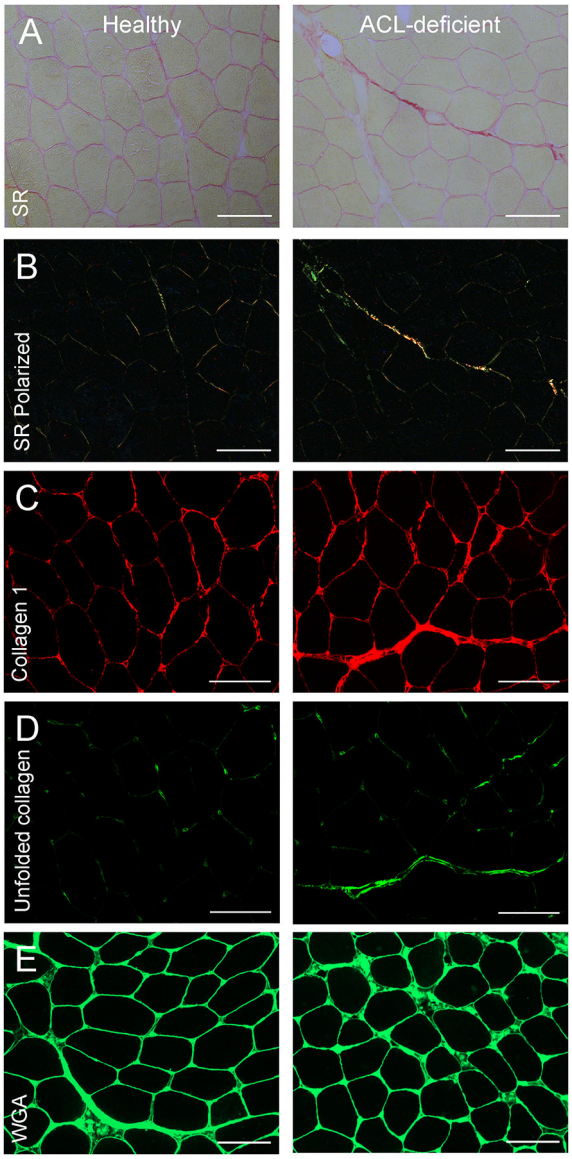

Figure 5. Representative images in the healthy and ACL-deficient quadriceps.

(A) Representative images of picro-sirius red staining of total collagen; (B) Representative images of picro-sirius red staining under circular polarized light (SR polarized); (C) Representative images of collagen 1 immunohistochemistry; (D) Representative images of collagen hybridizing peptide immunohistochemistry to ascertain unfolded collagen; (E) Representative images of wheat germ agglutinin staining to ascertain glycosaminoglycan content. Images were captured at 20X magnification at room temperature using a Zeiss upright microscope. Scale bar = 100μm. SR = picro-sirius red; SR polarized = picro-sirius red under circular polarized light; WGA = wheat germ agglutinin.

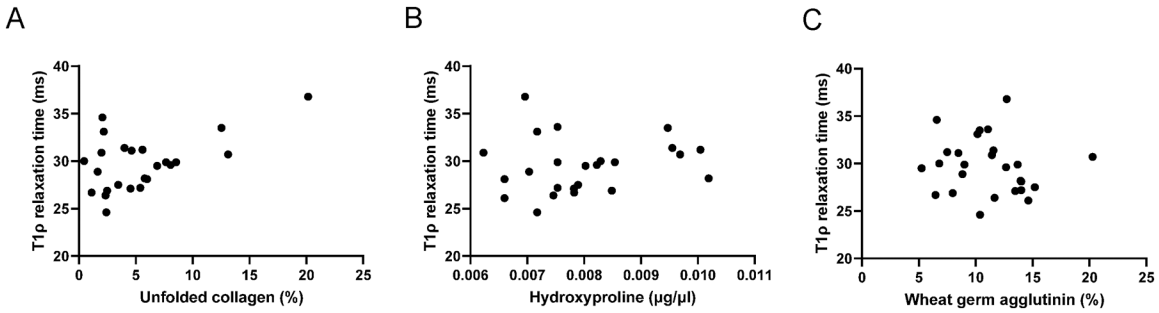

Figure 6. T1ρ relaxation time is positively associated with indices of unfolded collagen and hydroxyproline in ACL-deficient quadriceps muscle.

(A) Relationship between T1ρ relaxation time and unfolded collagen percent from the selected multiple linear regression model; (B) Relationship between T1ρ relaxation time and hydroxyproline from the selected multiple linear regression model;(C) Relationship between T1ρ relaxation time and glycosaminoglycan content estimated from wheat germ agglutinin staining from the selected multiple linear regression model. N=27 participants who underwent aligned T1ρ imaging and vastus lateralis biopsies.

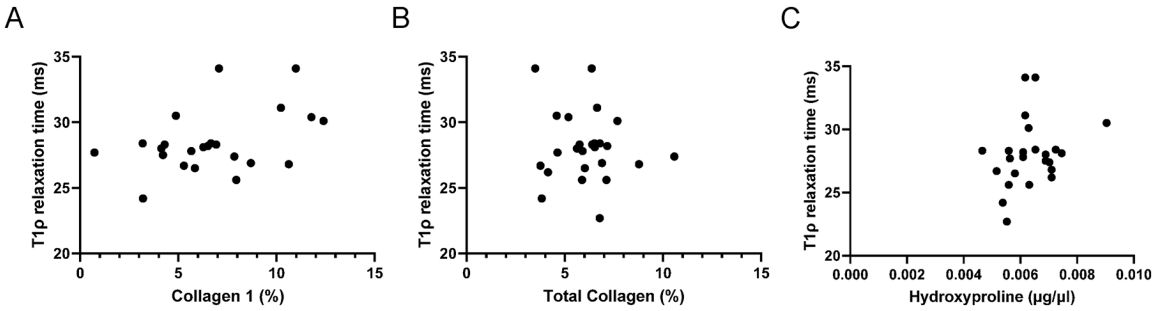

Figure 7. T1ρ relaxation time is positively associated with collagen abundance in healthy quadriceps muscle.

(A) Relationship between T1ρ relaxation time and collagen 1 content from the selected multiple linear regression model; (B) Relationship between T1ρ relaxation time and total collagen content from the selected multiple linear regression model; (C) Relationship between T1ρ relaxation time and hydroxyproline from the selected multiple linear regression model. N=27 participants who underwent aligned T1ρ imaging and vastus lateralis biopsies.

Table 1.

Candidate models predicting T1ρ relaxation time in ACL-deficient quadriceps

Number of Variables	Collagen 1 %	Unfolded Collagen %	Total Collagen %	Densely Organized Collagen (Natural Log)	Loosely Organized collagen (Natural log)	Wheat Germ Agglutinin %	Hydroxyproline (μg/μl)	R^2	Adjusted R^2
1		*						0.281	0.2486
1					*			0.166	0.1264
1	*							0.13	0.0907
1				*				0.03	−0.0161
1			*					0.035	−0.0087
2		*					*	0.427	0.3666
2		*				*		0.402	0.3446
2	*	*						0.306	0.2396
2					*	*		0.292	0.2214
2		*	*					0.281	0.2053
3		*****				*****	*****	**0.49**	**0.405**
3	*	*					*	0.447	0.3551
3				*	*	*		0.412	0.3186
3	*	*				*		0.414	0.3259
3		*	*			*		0.413	0.3147

Table 2.

Candidate models predicting T1ρ relaxation time in healthy quadriceps

Number of Variables	Collagen 1 %	Unfolded Collagen %	Total Collagen %	Densely Organized Collagen (Natural Log)	Loosely Organized collagen (Natural log)	Wheat Germ Agglutinin %	Hydroxyproline (μg/μl)	R^2	Adjusted R^2
1	*							0.147	0.108
1					*			0.144	0.094
1							*	0.077	0.035
1		*						0.066	0.024
1			*					0.012	−0.031
2	*				*			0.302	0.203
2	*			*				0.295	0.201
2	*		*					0.255	0.181
2					*		*	0.272	0.168
2	*						*	0.203	0.119
3	*****		*****				*****	**0.38**	**0.27**
3	*				*		*	0.401	0.237
3	*			*			*	0.384	0.23
3		*		*			*	0.367	0.209
3	*		*	*				0.347	0.208